Published in final edited form as:
Biochim Biophys Acta. 2014 July ; 1840(7): 2112–2122. doi:10.1016/j.bbagen.2014.03.008.

Choline kinase beta is required for normal endochondral bone formation

Zhuo Li[a], **Gengshu Wu**[a], **Roger B. Sher**[b], **Zohreh Khavandgar**[c], **Martin Hermansson**[a], **Gregory A. Cox**[d], **Michael R. Doschak**[e], **Monzur Murshed**[c,f], **Frank Beier**[g], and **Dennis E. Vance**[a]

[a]Group on the Molecular and Cell Biology of Lipids and Department of Biochemistry, University of Alberta, Edmonton, Alberta T6G 2S2 Canada

[b]University of Maine, Orono, ME USA

[c]Faculty of Dentistry, McGill University, Montreal, Quebec, Canada

[d]The Jackson Laboratory, Bar Harbor, Maine, USA

[e]Faculty of Pharmacy & Pharmaceutical Sciences, University of Alberta, Canada

[f]Department of Medicine, McGill University, Montreal, Quebec, Canada

[g]Department of Physiology and Pharmacology, Schulich School of Medicine and Dentistry University of Western Ontario, London, Ontario, Canada

Abstract

Background—Choline kinase has three isoforms encoded by the genes *Chka* and *Chkb*. Inactivation of *Chka* in mice results in embryonic lethality, whereas *Chkb*$^{-/-}$ mice display neonatal forelimb bone deformations.

Methods—To understand the mechanisms underlying the bone deformations, we compared the biology and biochemistry of bone formation from embryonic to young adult wild-type (WT) and *Chkb*$^{-/-}$ mice.

Results—The deformations are specific to the radius and ulna during the late embryonic stage. The radius and ulna of *Chkb*$^{-/-}$ mice display expanded hypertrophic zones, unorganized proliferative columns in their growth plates, and delayed formation of primary ossification centers. The differentiation of chondrocytes of *Chkb*$^{-/-}$ mice was impaired, as was chondrocyte proliferation and expression of matrix metalloproteinases 9 and 13. In chondrocytes from *Chkb*$^{-/-}$ mice, phosphatidylcholine was slightly lower than in WT mice whereas the amount of

[a]To whom correspondence should be addressed: Group on the Molecular and Cell Biology of Lipids, 328 HMRC, University of Alberta, Edmonton, Alberta, Canada T6G 2S2. dennis.vance@ualberta.ca, phone: 1-780-492-8286; fax: 1-780-492-3383.

Conflict of interests: the authors have no conflicts of interest or financial ties related to this manuscript.

phosphocholine was decreased by approximately 75%. In addition, the radius and ulna from *Chkb*$^{-/-}$ mice contained fewer osteoclasts along the cartilage/bone interface.

Conclusions—*Chkb* has a critical role in the normal embryogenic formation of the radius and ulna in mice.

Keywords

choline kinase; endochondral bone formation; growth plate; chondrocyte; radius; ulna; phosphocholine

1. Introduction

Choline kinase (CK) catalyzes the first reaction of the CDP-choline pathway, also known as the Kennedy pathway, for synthesis of phosphatidylcholine (PC), one of the major phospholipids in cellular membranes [1,2]. CK is a cytosolic enzyme, present in all tissues and converts choline to phosphocholine (PCho) [3]. CK exists in three isoforms in mice: CKα1 and CKα2 encoded by the *Chka* gene, and CKβ encoded by the *Chkb* gene. Active CK consists of either homo- or hetero-dimeric forms; neither isoform is active in its monomeric form [4].

Previous work demonstrated that *Chka* null mice die very early during embryonic development, indicating the importance of CK for embryonic development [5]. In 2006, mice with a spontaneous 1.6 kb intragenic deletion within the *Chkb* gene were identified [6]. The *Chkb*$^{-/-}$ mice have a rostral-to-caudal gradient of severity with minor forelimb but severe hindlimb muscular dystrophy. Previous work has shown that mitochondrial dysfunction contributes to the muscular dystrophy phenotype in *Chkb*$^{-/-}$ mice [7]. *Chkb*$^{-/-}$ mice also display striking bone deformation in the forelimb. However, the reason for the forelimb bone deformity had not been investigated.

The limb long bones form by endochondral ossification, during which a cartilage template is first formed and is subsequently replaced by bone tissue [8–12]. Endochondral bone formation begins with mesenchymal cell condensation that pre-figures the future shape of the bones. The cells in these mesenchymal condensations differentiate into chondrocytes, the major cell type in cartilage. This differentiation process is mainly regulated by the transcription factor Sox9 [13,14]. The chondrocytes then undergo proliferation that results in parallel columns of dividing cells. These dividing cells assume a flattened shape and form columns that resemble stacks of coins with a distinct orientation. The cells then stop dividing, exit from the cell cycle, increase in size and become mature and hypertrophic. The hypertrophic chondrocytes secrete a specialized extracellular matrix (ECM) which is eventually remodeled and digested by proteases. Two essential matrix metalloproteinases (MMPs), MMP9 and MMP13, are involved in the degradation of cartilage ECM [15–17]. Matrix degradation can facilitate the recruitment of blood vessels, as well as osteoblast and osteoclast cells to invade the hypertrophic cartilage for replacing it with mineralized bone tissue [18,19]. As bone enlarges further, a so-called secondary ossification center is established by a similar mechanism at the two ends of the bones. The cartilage structure between the two ossification centers is known as the growth plate. The growth plate consists

of distinct layers including the resting zone, proliferation zone and hypertrophic zone, and the longitudinal endochondral bone growth is primarily controlled by the growth plate activity [20,21].

In this study, we have demonstrated that *Chkb* plays an important role in endochondral bone formation and growth plate physiology. The endochondral bone formation defects and growth plate phenotypes of *Chkb*$^{-/-}$ mice significantly contribute to the forelimb bone deformity.

2. Materials and methods

2.1. Mouse breeding and genotyping

Chkb$^{-/-}$ mice in C57BL/6J background were originally generated at the Jackson Laboratory (Bar Harbor, Maine, USA) [6]. All animal procedures were approved by the University of Alberta's Institutional Animal Care Committee in accordance with guidelines of the Canadian Council on Animal Care. WT littermates were used as controls. Heterozygous mice were bred with each other so that litters and embryos of three genotypes were obtained. PCR genotyping was performed using DNA from digested tail samples. Two separate genotyping programs were used to amplify both the WT *Chkb* allele between exons 5 and 9 and the truncated *Chkb* allele between exons 3 and 11. The mutation identified in *Chkb*$^{-/-}$ mice is a 1.6 kb genomic deletion between exon 3 and intron 9 [6]. The primers used for genotyping were purchased from Integrated DNA Technologies (Coralville, IA, USA) and the sequences are included in Supplementary Table 1.

2.2. Skeletal stains and Micro-CT imaging

For staining of neonatal mouse skeleton and embryonic limb bones by Alizarin Red and Alcian Blue, the tissues were fixed overnight in 95% ethanol followed by overnight fixation in acetone. The tissues were then placed in staining solution for one week (0.05% Alizarin Red, 0.015% Alcian Blue, 5% acetic acid in 70% ethanol). The excess stain was cleared by treatment with 2% KOH followed by 1% KOH. Images of stained bones were obtained with an Olympus SP-57OUZ camera. The lengths of limb bones were measured in four littermate pairs using a dissecting microscope with a ruler. For Micro-CT imaging, intact mice and mouse forelimbs were scanned by Micro-CT (Skyscan 1076, Kontich, Belgium) at 9 μm resolution with 100 kV, 100 μA, and power of 10 W. Projected images of the samples were reconstructed using vendor supplied software (Nrecon 1.6.1.5, SkyScan NV, Kontich, Belgium).

2.3. Serum biochemistry and tissue-nonspecific alkaline phosphatase (TNAP) assay

Serum calcium level was measured using the QuantiChrom™ calcium assay kit (BioAssay Systems, Hayward, CA, USA). Insulin-like growth factor 1 (IGF-1) concentration in serum was measured using an IGF-1 immunoassay kit (R&D Systems, Minneapolis, MN, USA). Inorganic phosphate levels in serum, cells and tissues were measured by phosphate colorimetric assay kit (Abcam, Cambridge, MA, USA). Primary chondrocyte cell extracts were assayed for TNAP activity at 37 °C for 30 min using liquid *p*-nitrophenyl phosphate as substrate (Sigma-Aldrich, Oakville, ON, Canada). The colorimetric determination of the

product (*p*-nitrophenol) was performed at 405 nm and normalized to the amount of protein quantified by the Bradford method [22].

2.4. Histological analysis, tartrate-resistant acid phosphatase (TRAP) staining and immunohistochemistry

The long bones from new-born (P0) mice and embryos were dissected and fixed in 4% paraformaldehyde overnight. The tissues were then embedded in paraffin and 5 μm thick sections were prepared. Sections were de-waxed in xylene followed by graded dilutions of ethanol (100% twice, 95% once and 70% once) and finally water. For Safranin-O/fast green staining, tissue sections were stained in 0.01% fast green for 30 min, dipped in 1% acetic acid solution, then stained in 0.1% Safranin-O for 5 min. For von Kossa and van Gieson staining, the sections were stained in 1% silver nitrate solution, washed in distilled water, treated with 5% sodium thiosulfate, washed in tap water and finally van Gieson stain was applied. Tissue sections were dehydrated and coverslips were mounted using a xylene-based mounting solution. Growth plate morphology was examined with a Leica DMRA2 microscope equipped with a Retiga EX camera. The lengths of the hypertrophic zone and the whole growth plate were measured using OpenLab 4.0.4 software [23–25], and the ratio of the length of hypertrophic zone: the length of growth plate was calculated.

For immunohistochemistry, sections were incubated in 3% H_2O_2 for 15 min at room temperature, followed by antigen retrieval by incubation in 0.1% Triton X-100 for 13 min, followed by blocking with 5% goat or rabbit serum in phosphate-buffered saline. Sections were incubated with primary antibodies overnight at 4°C after which secondary antibodies were applied according to manufacturers' recommendations. Primary antibodies were: goat polyclonal anti-human Sox9 (AF3075, R&D Systems, Minneapolis, MN, USA) and mouse monoclonal anti-mouse proliferating cell nuclear antigen (PCNA) (2586S, Cell Signaling, Danvers, MA, USA). Incubation with horseradish peroxidase-conjugated secondary antibody (Abcam, Cambridge, MA, USA) was followed by colorimetric detection with the substrate diaminobenzidine (DAB) (Dako Canada Inc., Burlington, ON, Canada) Three independent stainings were performed and representative images are shown.

For TRAP staining, bone tissue sections from 7-day-old (P7) mice were stained to assess osteoclast numbers using a leukocyte acid phosphatase kit (Sigma-Aldrich, Oakville, ON, Canada). The staining was quantified by counting the number of positive foci along the chondro-osseous junction.

2.5. Primary culture of chondrocytes

Primary chondrocytes were prepared from long bones of embryonic 15.5-day-old (E15.5) mouse embryos, as previously described [26]. Briefly, the long bones were dissected and incubated at 37°C for 15 min in 0.25% trypsin-EDTA, followed by digestion at 37°C with 3 mg/ml collagenase P for 2 h in Dulbecco's modified Eagle's medium (DMEM) containing 10% fetal bovine serum (FBS). The cell suspensions were filtered through a 40 mm cell strainer (Fisher Scientific, Ottawa, ON, Canada), washed, counted and plated at 37°C in 6-well plates with media containing 2:3 DMEM:F12, 10% FBS, 0.5 mM L-glutamine, and penicillin/streptomycin (25 units/ml).

2.6. RNA isolation and quantitative real-time PCR analysis

RNA was isolated directly from either E15.5 embryonic bones or primary chondrocytes. For embryonic bones, E15.5 radius and ulna were dissected free from connective tissue. The bones were then placed into RNA stabilization reagent (Qiagen, Mississauga, ON, Canada) and passed through a series of syringes with 21G, 23G and 25G needles (BD Biosciences, Mississauga, ON, Canada) to break the tissues. The RNA in the homogenate was purified with RNeasy Micro Kit according to the manufacturer's instructions (Qiagen, Mississauga, ON, Canada). For primary chondrocytes, RNA was isolated using TRIzol reagent, then reverse-transcribed by oligo (dT) and Superscript II reverse transcriptase (Invitrogen, Burlington, ON, Canada). Quantitative real-time PCR was performed using a Rotor-Gene 3000 instrument and data were analyzed using the Rotor-Gene 6.0.19 software (Montreal Biotech, Dorval, QC, Canada). Cyclophilin mRNA was used to normalize gene expression. The primers (Supplementary Table 1) were purchased from Integrated DNA Technologies (Coralville, IA, USA).

2.7. Immunoblot analyses and choline kinase assay

For immunoblotting, primary chondrocyte cells were harvested in buffer containing 10 mM Tris-HCl (pH 7.2), 150 mM NaCl, 1 mM EDTA, 1 mM dithiothreitol, 1 mM phenylmethylsulfonyl fluoride and a protease inhibitor cocktail (1:100 dilution, P8340, Sigma-Aldrich, Oakville, ON, Canada). The cell extracts were centrifuged at 348,000 × *g* for 15 min at 4° C. The protein content of the supernatant (cytosol) was quantified by the Bradford procedure [22]. Proteins (50 μg/lane) were separated by electrophoresis on 10% polyacrylamide gels containing 0.1% SDS, and immunoblotted with the relevant primary antibodies. The following antibodies were used: rabbit polyclonal anti-mouse CKβ (dilution 1:1000; a gift from Dr. K. Ishidate, Teikyo Heisei University, Japan) and mouse monoclonal anti-rat Phospho1 (dilution 1:500, ab90581, Abcam, Cambridge, MA, USA). Antibodies raised against either α-tubulin or β-actin (Abcam, Cambridge, MA, USA) were used for loading controls.

Total CK activity was determined in the cytosolic fraction as described [27], with minor modifications. Briefly, the supernatants were incubated in a final volume of 100 μl buffer containing 0.1 M Tris-HCl, pH 8.75, 10 mM ATP, 15 mM $MgCl_2$, and 0.25 mM [^{3}H] choline chloride (10.5 μCi/ml) at 37 °C for 30 min. The product PCho was separated using an AG1-X8 (200–400 mesh, OH- form) column (Bio-Rad, Mississauga, ON, Canada).

2.8. Gelatin zymography

To determine MMP9 activity, primary chondrocyte cells were harvested in MMP lysis buffer (120 mM Tris, 0.1% Triton X-100, 0.01% NaN_3, 5% glycerol at pH 8.7). Proteins (10 μg/lane) were electrophoresed on SDS-polyacrylamide gels co-polymerized with gelatin (2 mg/ml). Distilled water and 20 μg proteins from the chondrogenic cell line ATDC5 (Sigma-Aldrich, Oakville, ON, Canada) were loaded onto the gel as negative and positive controls, respectively. Following electrophoresis, the gel was washed 4 times with 2.5% Triton X-100 for 15 min. MMP9 activity was developed by incubating the gel overnight at 37 °C in incubation buffer (50 mM Tris, 5 mM $CaCl_2$, 0.15 M NaCl, 0.5 mM NaN_3, pH 7.6) after which the gel was stained with Coomassie blue.

2.9. Mass-spectrometric analysis of lipids and water-soluble choline metabolites

Lipids were extracted from primary chondrocytes (100 μg protein) according to the method described in [28]. Phospholipid internal standards were used for quantification of the lipid species and were added at the stage of lipid extraction. The lipids were quantified using liquid chromatography-mass spectrometry (LC-MS) as described [29]. The acyl residues of the lipid species were quantified using fragmentation analysis [30]. The water-soluble choline metabolites were analyzed by LC-MS/MS as described previously [31].

2.10. Statistical analysis

All statistical analyses were performed using GraphPad Prism software 6.0. Data are mean values ± standard error of the mean (SEM). Statistical significance of differences ($P < 0.05$) was determined by the student's *t* test.

3. Results

3.1. Deformation of the radius and ulna in Chkb$^{-/-}$ mice

Fig. 1A shows the striking outward forelimb bone deformation of 7-day-old (P7) *Chkb*$^{-/-}$ mice. The forelimb bone deformation phenotype was also observed in newborn mice, and an initial characterization of this phenotype has been described [6]. To further characterize the forelimb bone deformity, the whole body and forelimbs of newborn (P0) *Chkb*$^{-/-}$ mice and WT littermates were stained with Alizarin Red & Alcian Blue and viewed by Micro-CT imaging. No gross skeletal abnormalities were observed except for the obvious deformations of the radius and ulna of the forelimb (Figs. 1B, C, D and E). No deformity of other limb long bones, including the humerus of the forelimb, was observed (Figs. 1C and 2C). To determine if the neonatal bone deformity persisted throughout the postnatal stage, the radius and ulna of 30-day-old (P30) mice were scanned by Micro-CT. The reconstructed image shows that the bone deformations in *Chkb*$^{-/-}$ mice become more severe over time and that the radius and ulna are curved almost to 90 degrees (Fig. 1F). Together, our observations revealed that the forelimb bone deformations in *Chkb*$^{-/-}$ mice are restricted to the radius and ulna and the deformities become more severe at later stages of development.

3.2. The radius and ulna in Chkb$^{-/-}$ mice are shorter than in WT mice and are deformed during embryonic development

To further characterize the limb long bones, the radius, ulna and humerus from the forelimb, and the tibia and femur from the hindlimb, of newborn mice were stained with Alizarin Red and Alcian Blue. In addition to the deformities, the lengths of the radius and ulna in neonatal *Chkb*$^{-/-}$ mice were significantly shorter than in WT mice, whereas the lengths of the humerus, tibia and femur were not different (Figs. 2A, C). However, in 21-day-old (P21) *Chkb*$^{-/-}$ mice, the humerus, tibia and femur were slightly shorter than in WT mice while the lengths of the radius and ulna were dramatically reduced (Supplementary Fig. 1C). Interestingly, the growth of *Chkb*$^{-/-}$ mice was also retarded, and these mice gained significantly less body weight before weaning (Supplementary Figs. 1A, B). The level of IGF-1, an important regulator of postnatal skeletal development [32,33], was approximately

50% lower in *Chkb*$^{-/-}$ mice than in WT mice (Supplementary Fig. 1D), which might contribute to the growth retardation.

The deformities of the radius and ulna in *Chkb*$^{-/-}$ mice are evident at birth, raising the possibility that their deformations occur during embryonic development. We, therefore, isolated and stained the forelimbs from E13.5 to E17.5 mice and observed deformations of the radius and ulna of *Chkb*$^{-/-}$ mice during late embryonic development (by E17.5) (Fig. 2B). The radius and ulna in *Chkb*$^{-/-}$ mice were shorter than in WT littermates as early as the E14.5 stage (Fig. 2B), suggesting that *Chkb*$^{-/-}$ mice have defects in embryonic cartilage development and that the bone shortening precedes the deformity.

3.3. The radius and ulna in Chkb$^{-/-}$ mice have growth plate defects

The presence of shorter embryonic and neonatal radius and ulna in the *Chkb*$^{-/-}$ mice suggests that the biology of their growth plates might be abnormal. Therefore, we studied the growth plate organization of the radius and ulna in P0 and E16.5 mice by Safranin O/fast green staining. Figure 3 shows representative images and quantification of the staining. The staining clearly shows that both the radius and ulna of *Chkb*$^{-/-}$ mice contain expanded hypertrophic zones (Figs. 3A, B). The ratio of hypertrophic zone length/total growth plate length also indicates that hypertrophic zones of the *Chkb*$^{-/-}$ mice are longer and enlarged compared to those in WT mice (~1.5 fold higher for the radius and ~2-fold higher for the ulna) (Figs. 3C, D). Moreover, the radius and ulna of E16.5 *Chkb*$^{-/-}$ mice also contained disorganized proliferation zones with loss of columnar organization and irregular chondrocyte morphology (Figs. 3E, F). Together, these observations clearly show that the radius and ulna of *Chkb*$^{-/-}$ mice have defects in growth plate development.

3.4. Impaired chondrocyte differentiation and decreased chondrocyte proliferation in the radius and ulna from Chkb$^{-/-}$ mice

The growth plate phenotypes observed in the radius and ulna of *Chkb*$^{-/-}$ mice suggest that endochondral bone formation is defective. We, therefore, examined chondrocyte differentiation and proliferation by immunohistochemistry of Sox9 and proliferating cell nuclear antigen (PCNA) expression in paraffin sections of E15.5 bones. Sox9 is an early chondrogenic marker that regulates chondrocyte differentiation [13,14]. The growth plates of both the radius and ulna of *Chkb*$^{-/-}$ mice exhibited significantly less Sox9 and PCNA expression than did of WT mice (Figs. 4A, B, D, and E). Quantification of the percentage of SOX9- and PCNA-expressing cells is shown in Figs. 4G and 4H, respectively. These data demonstrate that chondrocyte differentiation and proliferation of the radius and ulna are decreased in *Chkb*$^{-/-}$ mice. However, chondrocyte differentiation and proliferation of the humerus appear to be normal since Sox9 and PCNA expression is comparable to that in WT littermates (Figs. 4C, F, G and H).

3.5. MMP9 and MMP13 expression is impaired in the radius and ulna of Chkb$^{-/-}$ mice

Several MMPs are essential for the cleavage of cartilage ECM and replacement of cartilage by bone tissue. Loss of specific MMPs, such as MMP9 and MMP13, impairs matrix degradation and expands the hypertrophic zone in the growth plate [15–17]. Since the hypertrophic zones in the radius and ulna of *Chkb*$^{-/-}$ mice were enlarged, we studied

MMP9 and MMP13. We first performed quantitative real-time PCR gene expression analysis of the mRNAs encoded by *MMP9* and *MMP13* and observed significantly lower levels of *MMP9* and *MMP13* mRNAs in both embryonic bones and in primary chondrocytes in the radius and ulna of *Chkb*$^{-/-}$ mice compared to WT mice (Figs. 5A, B). We also performed gelatin zymography assays for MMP9 activity using primary chondrocytes isolated from the radius and ulna of E15.5 mice. MMP9 digests gelatin and exists in two forms: an uncleaved pro-form and a cleaved mature form [34]. Thus, MMP9 activity can be visualized as two bands after staining and destaining the gel. This assay showed that chondrocytes from the radius and ulna of *Chkb*$^{-/-}$ mice contained markedly less MMP9 activity than did those from WT mice (Fig. 5C). These data suggest that the radius and ulna from *Chkb*$^{-/-}$ mice have impaired MMP activity that leads to decreased cartilage ECM degradation.

3.6. Recruitment of osteoclasts to the chondro-osseous junction in the radius and ulna

Osteoclasts play an important role in endochondral ossification by cartilage resorption and the conversion of cartilage matrix to bone matrix [35]. Mice that are deficient in osteoclast production have enlarged hypertrophic zones in their growth plates [36]. Consequently, we determined if the growth plate phenotypes observed in *Chkb*$^{-/-}$ mice were associated with impaired cartilage resorption by staining P7 radius and ulna bone sections for tartrate-resistant acid phosphatase (TRAP). TRAP staining of the radius and ulna of *Chkb*$^{-/-}$ mice along the chondro-osseous junction was significantly less than that of the WT mice (Figs. 6A, B, C and D). The number of TRAP-positive foci in the radius and ulna was approximately 50% less in the *Chkb*$^{-/-}$ mice than in the WT mice (Figs. 6E, F). These data suggest that the recruitment of osteoclasts to the cartilage/bone junction is impaired in the radius and ulna of *Chkb*$^{-/-}$ mice.

3.7. Primary ossification of the radius and ulna

The aforementioned endochondral bone formation defects in the radius and ulna of *Chkb*$^{-/-}$ mice, including impaired ECM degradation and cartilage resorption, likely lead to delayed chondrocyte mineralization. We, therefore, determined if cartilage mineralization was altered by performing von Kossa staining of *Chkb*$^{-/-}$ and WT mice bone sections from the radius and ulna of E15.5 mice to examine the formation of primary ossification centers. Figure 7 shows that the mineralized area in the bone center of both the radius and ulna of *Chkb*$^{-/-}$ mice was smaller than in WT mice and that the zone of unmineralized cartilage was larger. These data indicate that formation of the primary ossification center of the radius and ulna of *Chkb*$^{-/-}$ mice is delayed. The enlargement of the hypertrophic zone and delayed cartilage mineralization are reminiscent of osteomalacia, a disease characterized by impaired bone mineralization, secondary to reduced plasma calcium levels [37]. However, serum calcium levels were not lower in *Chkb*$^{-/-}$ mice compared to WT mice (Supplementary Fig. 3C).

3.8. Biochemical analyses in primary chondrocytes

To confirm that CKβ had indeed been eliminated in the *Chkb*$^{-/-}$ mice, limb long bones from E15.5 mice were dissected free of soft tissue, and primary chondrocytes were isolated.

Immunoblotting confirmed the absence of CKβ in *Chkb*$^{-/-}$ mice (Fig. 8A). Moreover, total CK activity was approximately 80% lower in chondrocytes from all major long bones of *Chkb*$^{-/-}$ mice compared to WT mice (Fig. 8B). Because CK catalyzes the first step of the CDP-choline pathway for the synthesis of PC, we quantified the levels of choline metabolites and the major phospholipids in *Chkb*$^{-/-}$ and WT chondrocytes. Primary chondrocytes isolated from the combined radius and ulna, as well as from the humerus, were used for quantification of amounts of these metabolites by mass spectroscopy. Chondrocytes from the radius and ulna of *Chkb*$^{-/-}$ mice contained approximately 75% less PCho than those from WT mice whereas the amount of choline was not different (Fig. 8C). The amount of the phospholipid product, PC, was ~10% lower in chondrocytes from *Chkb*$^{-/-}$ compared to WT mice; amounts of other phospholipids were unchanged by CKβ deficiency (Fig. 8D). Similar to chondrocytes from the radius and ulna of *Chkb*$^{-/-}$ mice, the PCho level in chondrocytes from the humerus was also ~75% lower (Fig. 8E) whereas the amount of PC was decreased by only ~10% (Fig. 8F). Thus, the absence of CKβ in *Chkb*$^{-/-}$ mice only slightly reduces the amount of PC but significantly decreases PCho production in cartilage.

4. Discussion

These data show that the forelimb bone deformations in *Chkb*$^{-/-}$ mice are limited to the radius and ulna, and that the deformities occur before birth. Moreover, the radius and ulna of *Chkb*$^{-/-}$ mice have abnormal growth plate physiology and endochondral bone formation, including expanded hypertrophic zones, impaired chondrocyte differentiation and proliferation, decreased cartilage ECM digestion and osteoclast staining, and delayed formation of the primary ossification center.

4.1. Deformations of the radius and ulna of Chkb$^{-/-}$ mice are probably not caused by abnormal limb patterning

The initial phenotype characterized in *Chkb*$^{-/-}$ mice was muscular dystrophy; CKβ mutations have been identified in humans with muscular dystrophy [38]. However, no CKβ mutations in humans have been associated with bone disease. The radius and ulna deformations, and the growth retardation phenotype in *Chkb*$^{-/-}$ mice are reminiscent of Turner syndrome, Leri-Weill dyschondrosteosis and Langer syndrome in humans, which are associated with mutations in the short stature homeobox (Shox) gene. These individuals are characterized by dwarfism, limb shortening and bowed radius/ulna and tibia/fibula [39–41]. However, mice do not express the *Shox* gene [42] but do have the *Shox2* paralog, which is also expressed in humans [43]. *Shox2* deficiency in mice severely affects proximal limb development including that of the humerus and femur; in contrast, development of the radius and ulna is normal [44–46]. In *Chkb*$^{-/-}$ mice, the most prominent defects are in the radius and ulna. The formation and pattering of limbs are guided by Hox genes. Specific combinations of mutations in Hox genes result in severely deformed limb elements [47]. The formation and patterning of the radius and ulna are tightly regulated by Hoxa11 and Hoxd11. Inactivation of murine *Hoxa11* and *Hoxd11* completely disrupts formation of radius and ulna of the forelimb [48,49]. To determine if the deformations of the radius and ulna in *Chkb*$^{-/-}$ mice were due to altered *Hoxa11* and *Hoxd11* gene expression, we performed quantitative real-time PCR analysis of E15.5 embryonic bones and primary

chondrocytes from *Chkb*$^{-/-}$ and WT mice but did not detect any differences in expression of these two genes (Supplementary Fig. 2). This observation suggests that the deformities of the radius and ulna are probably not caused by abnormal limb patterning. This conclusion is also supported by the appearance of the deformities during late embryonic development (Fig. 2B), long after patterning has occurred.

4.2. Radius and ulna of Chkb$^{-/-}$ mice have impaired replacement of cartilage by bone

The most dramatic phenotypes observed in the growth plates of the radius and ulna from *Chkb*$^{-/-}$ mice are expanded hypertrophic zones (Fig. 3) and delayed formation of the primary ossification center (Fig. 7). These two growth plate defects suggest that CKβ deficiency impairs the conversion of cartilage to bone tissue. Cartilage matrix degradation plays an essential role in the replacement of cartilage by bone tissue. Invasion of the ossification front, including the formation of blood vessels, as well as osteoblast and osteoclast cells, requires extensive degradation of cartilage ECM surrounding the late hypertrophic cells. Two matrix proteinases, MMP9 and MMP13, are mainly responsible for the degradation of cartilage ECM. Mice deficient in either *MMP9* or *MMP13* have expanded hypertrophic zones and delayed primary endochondral ossification due to impeded digestion of ECM [15–17]. Interestingly, in *Chkb*$^{-/-}$ mice, *MMP9* and *MMP13* gene expression was significantly reduced in both embryonic radius and ulna, as well as in primary chondrocytes (Figs. 5A, B). The chondrocytes isolated from the radius and ulna of *Chkb*$^{-/-}$ mice also exhibited diminished MMP9 activity in vitro (Fig. 5C). These data suggest that ECM degradation is impaired in the radius and ulna of *Chkb*$^{-/-}$ mice, leading to slower conversion of cartilage into bone.

Osteoclasts are also important for establishment of primary ossification. In the absence of osteoclasts, cartilage ECM cannot be removed and there is no invasion by the ossification front or bone deposition on cartilage remnants. TRAP staining revealed that the radius and ulna of *Chkb*$^{-/-}$ mice recruit fewer osteoclasts to the cartilage/bone interface (Fig. 6), indicating decreased cartilage resorption by osteoclasts. These findings further support the conclusion that replacement of cartilage by bone in the radius and ulna is impaired in *Chkb*$^{-/-}$ mice. Previous studies showed that MMPs, particularly MMP9, are necessary for the migration of osteoclasts into hypertrophic cartilage during primary endochondral ossification [51,52].

4.3. Radius and ulna of Chkb$^{-/-}$ mice have impaired chondrocyte differentiation and decreased chondrocyte proliferation

In addition to the defects in endochondral bone formation discussed above, we demonstrated that the radius and ulna of *Chkb*$^{-/-}$ mice have impaired chondrocyte differentiation and decreased proliferation since the expression of Sox9 and PCNA was reduced in the growth plates (Figs. 4A, B, D, and E). Sox9 is an essential transcription factor that regulates the differentiation of chondrocytes from mesenchymal cells during chondrogenesis [13,14]. Haplo-insufficiency of *Sox9* in mice causes abnormalities in primordial cartilage including bending of the radius and ulna [52]. The decreased expression of Sox9 in the radius and ulna of embryonic *Chkb*$^{-/-}$ mice might be an important factor that contributes to the bending of these bones. Moreover, a reduction in chondrocyte proliferation is consistent with the

finding that bone lengths of the radius and ulna are reduced in *Chkb*$^{-/-}$ mice. Both CK and its product PCho have been implicated in cell proliferation and transformation [53–56]. Production of PCho is an important event in growth factor-induced mitogenesis in fibroblasts [57–59]. Moreover, increased CK activity has been detected in various cancer cells, and an elevated PCho level has been used as a biomarker for tumor diagnosis [60–63]. The amount of PCho in chondrocytes from the radius and ulna of *Chkb*$^{-/-}$ mice was significantly lower than in WT mice (Fig. 8C). Hence, the decrease in PCho might contribute to the growth defects in radius and ulna of *Chkb*$^{-/-}$ mice.

4.4. Conjecture of radius and ulna specific deformations

The reason why the bone deformities were restricted to radius and ulna in *Chkb*$^{-/-}$ mice, but did not occur in other limb bones, is unclear. Our previous work on the muscular dystrophy phenotype in *Chkb*$^{-/-}$ mice demonstrated that *Chkb* is the major CK isoform in the muscle of hindlimb but not forelimb [64]. This finding provides an explanation for why the muscle damage of *Chkb*$^{-/-}$ mice is more severe in the hindlimb than in the forelimb. Total CK activity in chondrocytes isolated from all the limb long bones of *Chkb*$^{-/-}$ mice was ~80% lower than in WT mice (Fig. 8B) suggesting that *Chkb* is the dominant isoform in chondrocytes from all the limb long bones. This observation appears to eliminate the possibility that the bone defects specifically in the radius and ulna are due to different expression levels of the CK isoforms in the radius/ulna versus other limb long bones. In addition, although our immunohistochemistry data for the humerus suggest that it has normal chondrocyte differentiation and proliferation (Figs. 4C, F, G, and H), we haven't fully examined other events of its endochondral bone formation. Other limb long bones in *Chkb*$^{-/-}$ mice including the humerus, tibia, and femur may have minor defects in some aspects of endochondral ossification and growth plate physiology, which, however, are probably not severe enough to induce the deformation. Perhaps, the unique anatomic feature of murine radius and ulna, that is, being located in the distal forelimb as well as being connected with each other to support the body weight, confer the fragility of deformity when CKβ is absent.

4.5. Absence of CKβ in Chkb$^{-/-}$ mice only slightly decreases PC but significantly reduces PCho in chondrocytes

In order to determine whether or not *Chkb* deficiency affected the amounts of choline metabolites and phospholipids in the cartilage of *Chkb*$^{-/-}$ mice, we isolated primary chondrocytes and quantified these metabolites by mass spectrometry. The PC content of chondrocytes from *Chkb*$^{-/-}$ mice was slightly lower than that of WT chondrocytes (Figs. 8D, F). This observation was not surprising since our previous studies have shown that the PC content of most tissues of *Chkb*$^{-/-}$ mice was not altered [6]. Moreover, the rate-limiting enzyme of the CDP-choline pathway for PC synthesis is CTP: phosphocholine cytidylyltransferase, rather than CK [2,65]. Thus, the bone defects in *Chkb*$^{-/-}$ mice are unlikely to be caused by a reduced content of PC. Nevertheless, the PCho content of chondrocytes from *Chkb*$^{-/-}$ mice was dramatically reduced, suggesting that the deficiency of PCho is more likely to be the cause of the bone defects (Figs. 8C, E). This reduction of PCho was expected since most intracellular PCho is produced from CK [2,66].

4.6. Other possible roles of decreased PCho in the phenotypes of Chkb $^{-/-}$ mice

In addition to a role for PCho in cell proliferation, PCho has also been implicated in regulating the function of Phospho1, a recently identified phosphatase that is expressed in the mineralization surface of both bone and cartilage [67]. Phospho1 plays an important role in skeletal calcification [68,69], and *Phospho1* knockout mice have decreased bone mineral density and deformed limb bones [70]. Phospho1 is a soluble cytosolic enzyme that has high phosphohydrolase activity towards PCho and phosphoethanolamine [71,72]. PCho and phosphoethanolamine are the two most abundant phospho-monoesters in cartilage [73]. CK also phosphorylates ethanolamine to phosphoethanolamine [74,75]. Possibly *Chkb* deficiency reduces the availability of substrates (PCho and phosphoethanolamine) for Phospho1 and thereby limits the ability of Phospho1 to produce sufficient inorganic phosphate (Pi) for cartilage mineralization. We observed that the amount of Phospho1 protein was higher in chondrocytes from *Chkb*$^{-/-}$ mice than in chondrocytes from WT mice (Supplementary Fig. 3A) suggesting that a compensatory mechanism is activated in response to lower substrate levels. Although the serum level of Pi is lower in *Chkb*$^{-/-}$ mice than in WT mice, the Pi content of both embryonic bone tissues and primary chondrocytes was not altered by CKβ deficiency (Supplementary Figs. 3D, E, F), suggesting that chondrocytes from *Chkb*$^{-/-}$ mice have sufficient Pi for normal mineralization. Indeed, the contribution of PCho and phosphoethanolamine to the total Pi pool is still unknown. Other phosphorus-containing molecules such as ATP, ADP and pyrophosphate are also important sources of Pi. All of these molecules are hydrolyzed by the major phosphatase in skeletal tissue, the tissue non-specific alkaline phosphatase (TNAP) [76–78]. Our experiments showed that TNAP activity in chondrocytes from *Chkb*$^{-/-}$ mice was the same as in WT chondrocytes (Supplementary Fig. 3B). Furthermore, the staining and Micro-CT images of skeletons did not reveal any obvious calcification defects in *Chkb*$^{-/-}$ mice (Fig. 1). Therefore, we propose that the delay in cartilage mineralization in the radius and ulna of *Chkb*$^{-/-}$ mice is primarily due to slower replacement of cartilage by bone rather than defects in mineralization capability.

Although the majority of PCho is produced by the CK reaction, some PCho (along with ceramide) is generated from sphingomyelin by the neutral sphingomyelinase 2 (nSMase2), which is encoded by the *Smpd3* gene. *Smpd3*-deficient mice display dwarfism, chondrodysplasia, limb bone deformation and abnormal embryonic growth plate phenotypes [79–82]. These features are similar to those exhibited by *Chkb*$^{-/-}$ mice. In addition, *Smpd3*-deficient mice also show severe hypomineralization pathology [79,82], which is not observed in the *Chkb*$^{-/-}$ mice in this study. The role that PCho and/or ceramide plays in the bone phenotypes of *Smpd3*-deficient mice is still unknown.

In conclusion, our data show that *Chkb*$^{-/-}$ mice have bone deformations specifically in the radius and ulna and that these defects occur during late embryonic development. *Chkb* deficiency in chondrocytes leads to a dramatic reduction in the amount of PCho but only a slight decrease of PC. The radius and ulna of *Chkb*$^{-/-}$ mice have several defects in endochondral bone formation including abnormal growth plate organization, decreased chondrocyte differentiation and proliferation, impaired ECM degradation, reduced osteoclast recruitment and delayed cartilage mineralization. These combined defects in cartilage

development significantly contribute to the deformities of the radius and ulna. To our knowledge this is the first study to demonstrate that *Chkb* plays an essential role in endochondral bone formation, at least in the radius and ulna. Future studies on tissue-specific inactivation of *Chkb*, or even *Chka*, in cartilage, osteoblasts or osteoclasts are likely to provide additional novel insights into the role of CK in normal endochondral bone formation.

Supplementary Material

Refer to Web version on PubMed Central for supplementary material.

Acknowledgments

We appreciate the excellent technical assistance from Susanne Lingrell and Randy Nelson. We would like to thank all members of Dr. Frank Beier's lab at University of Western Ontario (Canada) for training in techniques including skeletal staining, immunohistochemistry and preparation of primary chondrocytes, and for providing the Sox9 and PCNA antibodies used in our study. We are grateful to Dr. Jean Vance for suggestions on the manuscript. M.H. is a fellow of the Sigrid Jusélius Foundation. G.A.C. and R.B.S. were supported by the National Institute of Arthritis and Musculoskeletal and Skin Diseases of the National Institutes of Health under Award Number AR054170. This research was supported by a grant (MOP5182) from the Canadian Institutes of Health Research.

Abbreviations

CK	choline kinase
DMEM	Dulbecco's modified Eagle's medium
ECM	extracellular matrix
FBS	fetal bovine serum
IGF-1	insulin-like growth factor 1
LC-MS	liquid chromatography-mass spectrometry
MMP	matrix metalloproteinase
PC	phosphatidylcholine
PCho	phosphocholine
PCNA	proliferating cell nuclear antigen
TNAP	tissue-nonspecific alkaline phosphatase
TRAP	tartrate-resistant acid phosphatase

References

1. Vance, DE.; Vance, JE. Phospholipid biosynthesis in eukaryotes. In: Vance, DE.; Vance, JE., editors. Biochemistry of Lipids, Lipoproteins, and Membranes. 5th Edition. Amsterdam: Elsevier; 2008. p. 213-244.
2. Kennedy EP. Metabolism of lipides. Annu Rev Biochem. 1957; 26:119–148. [PubMed: 13488391]
3. Wittenberg J, Kornberg A. Choline phosphokinase. J Biol Chem. 1953; 202:431–444. [PubMed: 13061469]
4. Aoyama C, Liao H, Ishidate K. Structure and function of choline kinase isoforms in mammalian cells. Prog Lipid Res. 2004; 43:266–281. [PubMed: 15003397]

5. Wu G, Aoyama C, Young SG, Vance DE. Early embryonic lethality caused by disruption of the gene for choline kinase alpha, the first enzyme in phosphatidylcholine biosynthesis. J Biol Chem. 2008; 283:1456–1462. [PubMed: 18029352]
6. Sher RB, Aoyama C, Huebsch KA, Ji S, Kerner J, Yang Y, Frankel WN, Hoppel CL, Wood PA, Vance DE, Cox GA. A rostrocaudal muscular dystrophy caused by a defect in choline kinase beta, the first enzyme in phosphatidylcholine biosynthesis. J Biol Chem. 2006; 281:4938–4948. [PubMed: 16371353]
7. Wu G, Sher RB, Cox GA, Vance DE. Understanding the muscular dystrophy caused by deletion of choline kinase beta in mice. Biochim Biophys Acta. 2009; 1791:347–356. [PubMed: 19236939]
8. Olsen BR, Reginato AM, Wang W. Bone development. Annu Rev Cell Dev Biol. 2000; 16:191–220. [PubMed: 11031235]
9. Karsenty G, Wagner EF. Reaching a genetic and molecular understanding of skeletal development. Dev Cell. 2002; 2:389–406. [PubMed: 11970890]
10. Kronenberg HM. Developmental regulation of the growth plate. Nature. 2003; 423:332–336. [PubMed: 12748651]
11. Provot S, Schipani E. Molecular mechanisms of endochondral bone development. Biochem Biophys Res Commun. 2005; 328:658–665. [PubMed: 15694399]
12. Mackie EJ, Ahmed YA, Tatarczuch L, Chen KS, Mirams M. Endochondral ossification: how cartilage is converted into bone in the developing skeleton. Int J Biochem Cell Biol. 2008; 40:46–62. [PubMed: 17659995]
13. Bi W, Deng JM, Zhang Z, Behringer RR, de Crombrugghe B. Sox9 is required for cartilage formation. Nat Genet. 1999; 22:85–89. [PubMed: 10319868]
14. Akiyama H, Chaboissier MC, Martin JF, Schedl A, de Crombrugghe B. The transcription factor Sox9 has essential roles in successive steps of the chondrocyte differentiation pathway and is required for expression of Sox5 and Sox6. Genes Dev. 2002; 16:2813–2828. [PubMed: 12414734]
15. Vu TH, Shipley JM, Bergers G, Berger JE, Helms JA, Hanahan D, Shapiro SD, Senior RM, Werb Z. MMP-9/gelatinase B is a key regulator of growth plate angiogenesis and apoptosis of hypertrophic chondrocytes. Cell. 1998; 93:411–422. [PubMed: 9590175]
16. Inada M, Wang Y, Byrne MH, Rahman MU, Miyaura C, Lopez-Otin C, Krane SM. Critical roles for collagenase-3 (Mmp13) in development of growth plate cartilage and in endochondral ossification. Proc Natl Acad Sci U S A. 2004; 101:17192–17197. [PubMed: 15563592]
17. Stickens D, Behonick DJ, Ortega N, Heyer B, Hartenstein B, Yu Y, Fosang AJ, Schorpp-Kistner M, Angel P, Werb Z. Altered endochondral bone development in matrix metalloproteinase 13-deficient mice. Development. 2004; 131:5883–5895. [PubMed: 15539485]
18. Ortega N, Behonick D, Stickens D, Werb Z. How proteases regulate bone morphogenesis. Ann N Y Acad Sci. 2003; 995:109–116. [PubMed: 12814943]
19. Ortega N, Behonick DJ, Werb Z. Matrix remodeling during endochondral ossification. Trends Cell Biol. 2004; 14:86–93. [PubMed: 15102440]
20. Ballock RT, O'Keefe RJ. Physiology and pathophysiology of the growth plate. Birth Defects Res C Embryo Today. 2003; 69:123–143. [PubMed: 12955857]
21. Beier F. Cell-cycle control and the cartilage growth plate. J Cell Physiol. 2005; 202:1–8. [PubMed: 15389526]
22. Bradford MM. A rapid and sensitive method for the quantitation of microgram quantities of protein utilizing the principle of protein-dye binding. Anal Biochem. 1976; 72:248–254. [PubMed: 942051]
23. Wang G, Woods A, Agoston H, Ulici V, Glogauer M, Beier F. Genetic ablation of Rac1 in cartilage results in chondrodysplasia. Dev Biol. 2007; 306:612–623. [PubMed: 17467682]
24. Ulici V, Hoenselaar KD, Agoston H, McErlain DD, Umoh J, Chakrabarti S, Holdsworth DW, Beier F. The role of Akt1 in terminal stages of endochondral bone formation: angiogenesis and ossification. Bone. 2009; 45:1133–1145. [PubMed: 19679212]
25. Usmani SE, Pest MA, Kim G, Ohora SN, Qin L, Beier F. Transforming growth factor alpha controls the transition from hypertrophic cartilage to bone during endochondral bone growth. Bone. 2012; 51:131–141. [PubMed: 22575362]

26. James CG, Woods A, Underhill TM, Beier F. The transcription factor ATF3 is upregulated during chondrocyte differentiation and represses cyclin D1 and A gene transcription. BMC Mol Biol. 2006; 7:30. [PubMed: 16984628]
27. Ishidate K, Nakazawa Y. Choline/ethanolamine kinase from rat kidney. Methods Enzymol. 1992; 209:121–134. [PubMed: 1323025]
28. Folch J, Lees M, Sloane Stanley GH. A simple method for the isolation and purification of total lipides from animal tissues. J Biol Chem. 1957; 226:497–509. [PubMed: 13428781]
29. Hermansson M, Uphoff A, Kakela R, Somerharju P. Automated quantitative analysis of complex lipidomes by liquid chromatography/mass spectrometry. Anal Chem. 2005; 77:2166–2175. [PubMed: 15801751]
30. Kainu V, Hermansson M, Somerharju P. Electrospray ionization mass spectrometry and exogenous heavy isotope-labeled lipid species provide detailed information on aminophospholipid acyl chain remodeling. J Biol Chem. 2008; 283:3676–3687. [PubMed: 18056998]
31. Xiong Y, Zhao YY, Goruk S, Oilund K, Field CJ, Jacobs RL, Curtis JM. Validation of an LC-MS/MS method for the quantification of choline-related compounds and phospholipids in foods and tissues. J Chromatogr B Analyt Technol Biomed Life Sci. 2012; 911:170–179.
32. Baker J, Liu JP, Robertson EJ, Efstratiadis A. Role of insulin-like growth factors in embryonic and postnatal growth. Cell. 1993; 75:73–82. [PubMed: 8402902]
33. Yakar S, Rosen CJ, Beamer WG, Ackert-Bicknell CL, Wu Y, Liu JL, Ooi GT, Setser J, Frystyk J, Boisclair YR, LeRoith D. Circulating levels of IGF-1 directly regulate bone growth and density. J Clin Invest. 2002; 110:771–781. [PubMed: 12235108]
34. Krane SM, Inada M. Matrix metalloproteinases and bone. Bone. 2008; 43:7–18. [PubMed: 18486584]
35. Novack DV, Teitelbaum SL. The osteoclast: friend or foe? Annu Rev Pathol. 2008; 3:457–484. [PubMed: 18039135]
36. Ortega N, Wang K, Ferrara N, Werb Z, Vu TH. Complementary interplay between matrix metalloproteinase-9, vascular endothelial growth factor and osteoclast function drives endochondral bone formation. Dis Model Mech. 2010; 3:224–235. [PubMed: 20142327]
37. Yoshida T, Stern PH. How vitamin D works on bone. Endocrinol Metab Clin North Am. 2012; 41:557–569. [PubMed: 22877429]
38. Mitsuhashi S, Nishino I. Megaconial congenital muscular dystrophy due to loss-of-function mutations in choline kinase beta. Curr Opin Neurol. 2013; 26:536–543. [PubMed: 23945283]
39. Rao E, Weiss B, Fukami M, Rump A, Niesler B, Mertz A, Muroya K, Binder G, Kirsch S, Winkelmann M, Nordsiek G, Heinrich U, Breuning MH, Ranke MB, Rosenthal A, Ogata T, Rappold GA. Pseudoautosomal deletions encompassing a novel homeobox gene cause growth failure in idiopathic short stature and Turner syndrome. Nat Genet. 1997; 16:54–63. [PubMed: 9140395]
40. Munns CF, Glass IA, LaBrom R, Hayes M, Flanagan S, Berry M, Hyland VJ, Batch JA, Philips GE, Vickers D. Histopathological analysis of Leri-Weill dyschondrosteosis: disordered growth plate. Hand Surg. 2001; 6:13–23. [PubMed: 11677662]
41. Zinn AR, Wei F, Zhang L, Elder FF, Scott CI Jr, Marttila P, Ross JL. Complete SHOX deficiency causes Langer mesomelic dysplasia. Am J Med Genet. 2002; 110:158–163. [PubMed: 12116254]
42. Gianfrancesco F, Sanges R, Esposito T, Tempesta S, Rao E, Rappold G, Archidiacono N, Graves JA, Forabosco A, D'Urso M. Differential divergence of three human pseudoautosomal genes and their mouse homologs: implications for sex chromosome evolution. Genome Res. 2001; 11:2095–2100. [PubMed: 11731500]
43. Clement-Jones M, Schiller S, Rao E, Blaschke RJ, Zuniga A, Zeller R, Robson SC, Binder G, Glass I, Strachan T, Lindsay S, Rappold GA. The short stature homeobox gene SHOX is involved in skeletal abnormalities in Turner syndrome. Hum Mol Genet. 2000; 9:695–702. [PubMed: 10749976]
44. Cobb J, Dierich A, Huss-Garcia Y, Duboule D. A mouse model for human short-stature syndromes identifies Shox2 as an upstream regulator of Runx2 during long-bone development. Proc Natl Acad Sci U S A. 2006; 103:4511–4515. [PubMed: 16537395]

45. Yu L, Liu H, Yan M, Yang J, Long F, Muneoka K, Chen Y. Shox2 is required for chondrocyte proliferation and maturation in proximal limb skeleton. Dev Biol. 2007; 306:549–559. [PubMed: 17481601]
46. Vickerman L, Neufeld S, Cobb J. Shox2 function couples neural, muscular and skeletal development in the proximal forelimb. Dev Biol. 2011; 350:323–336. [PubMed: 21156168]
47. Zeller R, Lopez-Rios J, Zuniga A. Vertebrate limb bud development: moving towards integrative analysis of organogenesis. Nat Rev Genet. 2009; 10:845–858. [PubMed: 19920852]
48. Davis AP, Witte DP, Hsieh-Li HM, Potter SS, Capecchi MR. Absence of radius and ulna in mice lacking hoxa-11 and hoxd-11. Nature. 1995; 375:791–795. [PubMed: 7596412]
49. Boulet AM, Capecchi MR. Multiple roles of Hoxa11 and Hoxd11 in the formation of the mammalian forelimb zeugopod. Development. 2004; 131:299–309. [PubMed: 14668414]
50. Blavier L, Delaisse JM. Matrix metalloproteinases are obligatory for the migration of preosteoclasts to the developing marrow cavity of primitive long bones. J Cell Sci. 1995; 108(Pt 12):3649–3659. [PubMed: 8719871]
51. Engsig MT, Chen QJ, Vu TH, Pedersen AC, Therkidsen B, Lund LR, Henriksen K, Lenhard T, Foged NT, Werb Z, Delaisse JM. Matrix metalloproteinase 9 and vascular endothelial growth factor are essential for osteoclast recruitment into developing long bones. J Cell Biol. 2000; 151:879–889. [PubMed: 11076971]
52. Bi W, Huang W, Whitworth DJ, Deng JM, Zhang Z, Behringer RR, de Crombrugghe B. Haploinsufficiency of Sox9 results in defective cartilage primordia and premature skeletal mineralization. Proc Natl Acad Sci U S A. 2001; 98:6698–6703. [PubMed: 11371614]
53. Lacal JC. Choline kinase: a novel target for antitumor drugs. IDrugs. 2001; 4:419–426. [PubMed: 16015482]
54. Rodriguez-Gonzalez A, Ramirez de Molina A, Benitez-Rajal J, Lacal JC. Phospholipase D and choline kinase: their role in cancer development and their potential as drug targets. Prog Cell Cycle Res. 2003; 5:191–201. [PubMed: 14593713]
55. Glunde K, Bhujwalla ZM, Ronen SM. Choline metabolism in malignant transformation. Nat Rev Cancer. 2011; 11:835–848. [PubMed: 22089420]
56. Gallego-Ortega D, Gomez del Pulgar T, Valdes-Mora F, Cebrian A, Lacal JC. Involvement of human choline kinase alpha and beta in carcinogenesis: a different role in lipid metabolism and biological functions. Adv Enzyme Regul. 2011; 51:183–194. [PubMed: 21035492]
57. Cuadrado A, Carnero A, Dolfi F, Jimenez B, Lacal JC. Phosphorylcholine: a novel second messenger essential for mitogenic activity of growth factors. Oncogene. 1993; 8:2959–2968. [PubMed: 8414498]
58. Jimenez B, del Peso L, Montaner S, Esteve P, Lacal JC. Generation of phosphorylcholine as an essential event in the activation of Raf-1 and MAP-kinases in growth factors-induced mitogenic stimulation. J Cell Biochem. 1995; 57:141–149. [PubMed: 7721953]
59. Kiss Z, Chung T. Choline phosphate and phorbol ester potentiate the mitogenic effect of insulin by competitive mechanisms in NIH 3T3 fibroblasts. Biochem Biophys Res Commun. 1996; 218:505–509. [PubMed: 8561786]
60. Nakagami K, Uchida T, Ohwada S, Koibuchi Y, Suda Y, Sekine T, Morishita Y. Increased choline kinase activity and elevated phosphocholine levels in human colon cancer. Jpn J Cancer Res. 1999; 90:419–424. [PubMed: 10363580]
61. Ramirez de Molina A, Rodriguez-Gonzalez A, Gutierrez R, Martinez-Pineiro L, Sanchez J, Bonilla F, Rosell R, Lacal J. Overexpression of choline kinase is a frequent feature in human tumor-derived cell lines and in lung, prostate, and colorectal human cancers. Biochem Biophys Res Commun. 2002; 296:580–583. [PubMed: 12176020]
62. Ramirez de Molina A, Sarmentero-Estrada J, Belda-Iniesta C, Taron M, Ramirez de Molina V, Cejas P, Skrzypski M, Gallego-Ortega D, de Castro J, Casado E, Garcia-Cabezas MA, Sanchez JJ, Nistal M, Rosell R, Gonzalez-Baron M, Lacal JC. Expression of choline kinase alpha to predict outcome in patients with early-stage non-small-cell lung cancer: a retrospective study. Lancet Oncol. 2007; 8:889–897. [PubMed: 17851129]
63. Eliyahu G, Kreizman T, Degani H. Phosphocholine as a biomarker of breast cancer: molecular and biochemical studies. Int J Cancer. 2007; 120:1721–1730. [PubMed: 17236204]

64. Wu G, Sher RB, Cox GA, Vance DE. Differential expression of choline kinase isoforms in skeletal muscle explains the phenotypic variability in the rostrocaudal muscular dystrophy mouse. Biochimica et biophysica acta. 2010; 1801:446–454. [PubMed: 20026284]

65. Kent C. Regulation of phosphatidylcholine biosynthesis. Prog Lipid Res. 1990; 29:87–105. [PubMed: 1965552]

66. Vance DE. Boehringer Mannheim Award lecture. Phosphatidylcholine metabolism: masochistic enzymology, metabolic regulation, and lipoprotein assembly. Biochem Cell Biol. 1990; 68:1151–1165. [PubMed: 2268410]

67. Houston B, Stewart AJ, Farquharson C. PHOSPHO1-A novel phosphatase specifically expressed at sites of mineralisation in bone and cartilage. Bone. 2004; 34:629–637. [PubMed: 15050893]

68. Stewart AJ, Roberts SJ, Seawright E, Davey MG, Fleming RH, Farquharson C. The presence of PHOSPHO1 in matrix vesicles and its developmental expression prior to skeletal mineralization. Bone. 2006; 39:1000–1007. [PubMed: 16837257]

69. Roberts S, Narisawa S, Harmey D, Millan JL, Farquharson C. Functional involvement of PHOSPHO1 in matrix vesicle-mediated skeletal mineralization. J Bone Miner Res. 2007; 22:617–627. [PubMed: 17227223]

70. Yadav MC, Simao AM, Narisawa S, Huesa C, McKee MD, Farquharson C, Millan JL. Loss of skeletal mineralization by the simultaneous ablation of PHOSPHO1 and alkaline phosphatase function: a unified model of the mechanisms of initiation of skeletal calcification. J Bone Miner Res. 2011; 26:286–297. [PubMed: 20684022]

71. Roberts SJ, Stewart AJ, Sadler PJ, Farquharson C. Human PHOSPHO1 exhibits high specific phosphoethanolamine and phosphocholine phosphatase activities. Biochem J. 2004; 382:59–65. [PubMed: 15175005]

72. Roberts SJ, Stewart AJ, Schmid R, Blindauer CA, Bond SR, Sadler PJ, Farquharson C. Probing the substrate specificities of human PHOSPHO1 and PHOSPHO2. Biochimica et biophysica acta. 2005; 1752:73–82. [PubMed: 16054448]

73. Kvam BJ, Pollesello P, Vittur F, Paoletti S. 31P NMR studies of resting zone cartilage from growth plate. Magn Reson Med. 1992; 25:355–361. [PubMed: 1614320]

74. Porter TJ, Kent C. Purification and characterization of choline/ethanolamine kinase from rat liver. J Biol Chem. 1990; 265:414–422. [PubMed: 2152925]

75. Aoyama C, Nakashima K, Ishidate K. Molecular cloning of mouse choline kinase and choline/ethanolamine kinase: their sequence comparison to the respective rat homologs. Biochimica et biophysica acta. 1998; 1393:179–185. [PubMed: 9714798]

76. Moss DW, Eaton RH, Smith JK, Whitby LG. Association of inorganic-pyrophosphatase activity with human alkaline-phosphatase preparations. Biochem J. 1967; 102:53–57. [PubMed: 6030299]

77. Majeska RJ, Wuthier RE. Studies on matrix vesicles isolated from chick epiphyseal cartilage. Association of pyrophosphatase and ATPase activities with alkaline phosphatase. Biochimica et biophysica acta. 1975; 391:51–60. [PubMed: 237558]

78. Anderson HC. Molecular biology of matrix vesicles. Clin Orthop Relat Res. 1995:266–280. [PubMed: 7634645]

79. Aubin I, Adams CP, Opsahl S, Septier D, Bishop CE, Auge N, Salvayre R, Negre-Salvayre A, Goldberg M, Guenet JL, Poirier C. A deletion in the gene encoding sphingomyelin phosphodiesterase 3 (Smpd3) results in osteogenesis and dentinogenesis imperfecta in the mouse. Nat Genet. 2005; 37:803–805. [PubMed: 16025116]

80. Stoffel W, Jenke B, Block B, Zumbansen M, Koebke J. Neutral sphingomyelinase 2 (smpd3) in the control of postnatal growth and development. Proc Natl Acad Sci U S A. 2005; 102:4554–4559. [PubMed: 15764706]

81. Stoffel W, Jenke B, Holz B, Binczek E, Gunter RH, Knifka J, Koebke J, Niehoff A. Neutral sphingomyelinase (SMPD3) deficiency causes a novel form of chondrodysplasia and dwarfism that is rescued by Col2A1-driven smpd3 transgene expression. Am J Pathol. 2007; 171:153–161. [PubMed: 17591962]

82. Khavandgar Z, Poirier C, Clarke CJ, Li J, Wang N, McKee MD, Hannun YA, Murshed M. A cell-autonomous requirement for neutral sphingomyelinase 2 in bone mineralization. J Cell Biol. 2011; 194:277–289. [PubMed: 21788370]

General Significance

Our data indicate that choline kinase beta plays an important role in endochondral bone formation by modulating growth plate physiology.

Highlights

- We characterized the forelimb bone deformities in *Chkb*$^{-/-}$ mice.
- The radius and ulna of *Chkb*$^{-/-}$ mice have abnormal growth plate physiology.
- The radius and ulna of *Chkb*$^{-/-}$ mice have endochondral bone formation defects.
- Phosphocholine but not phosphatidylcholine is dramatically reduced in *Chkb*$^{-/-}$ mice.

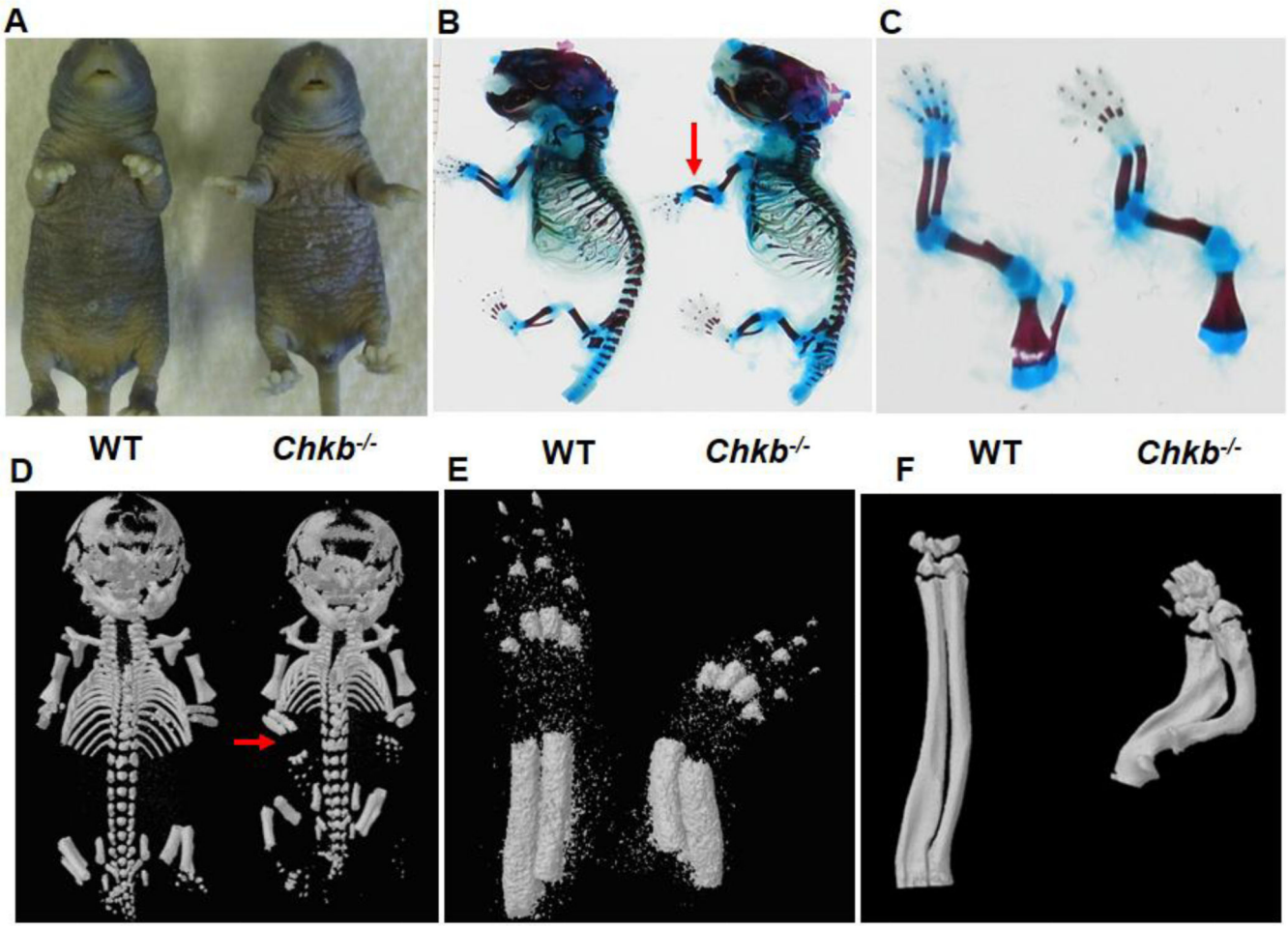

Fig. 1.

Deformation of the radius and ulna in *Chkb*$^{-/-}$ mice. Outward rotational forelimb bone deformation was examined in P7 WT and *Chkb*$^{-/-}$ mice (A). Radius and ulna deformations in P0 mice were visualized by skeletal staining of whole body (B) and forelimbs (C) with Alizarin Red and Alcian Blue. Micro-CT imaging was performed on whole body (D) and forelimbs (E). Severe deformation of the radius and ulna in 30-day-old *Chkb*$^{-/-}$ mice was visualized by Micro-CT imaging (F). Red arrows indicate deformed radius and ulna in (B) and (D).

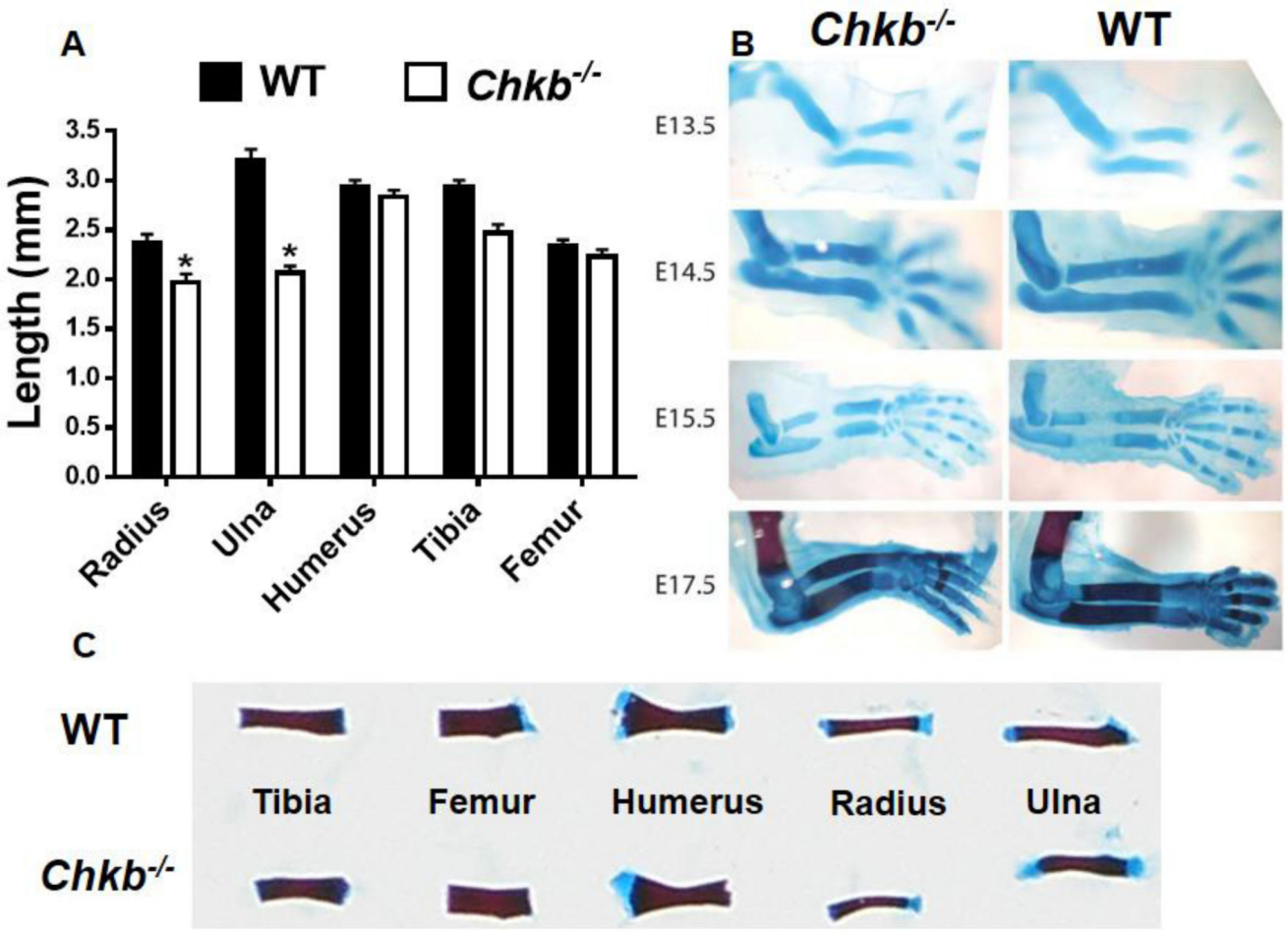

Fig. 2.

Length of radius and ulna and bone deformation during embryonic development. Long bones from newborn (P0) mice were dissected, stained with Alizarin Red and Alcian Blue and the bone lengths were measured (A, C). Data in (A) are means ± SEM from 4 littermates of each genotype; *: $P < 0.05$ compared to WT. Forelimbs were dissected free from soft tissues. E13.5-E15.5 forelimbs were stained with Alcian Blue only whereas E17.5 forelimbs were stained with both Alizarin Red and Alcian Blue.

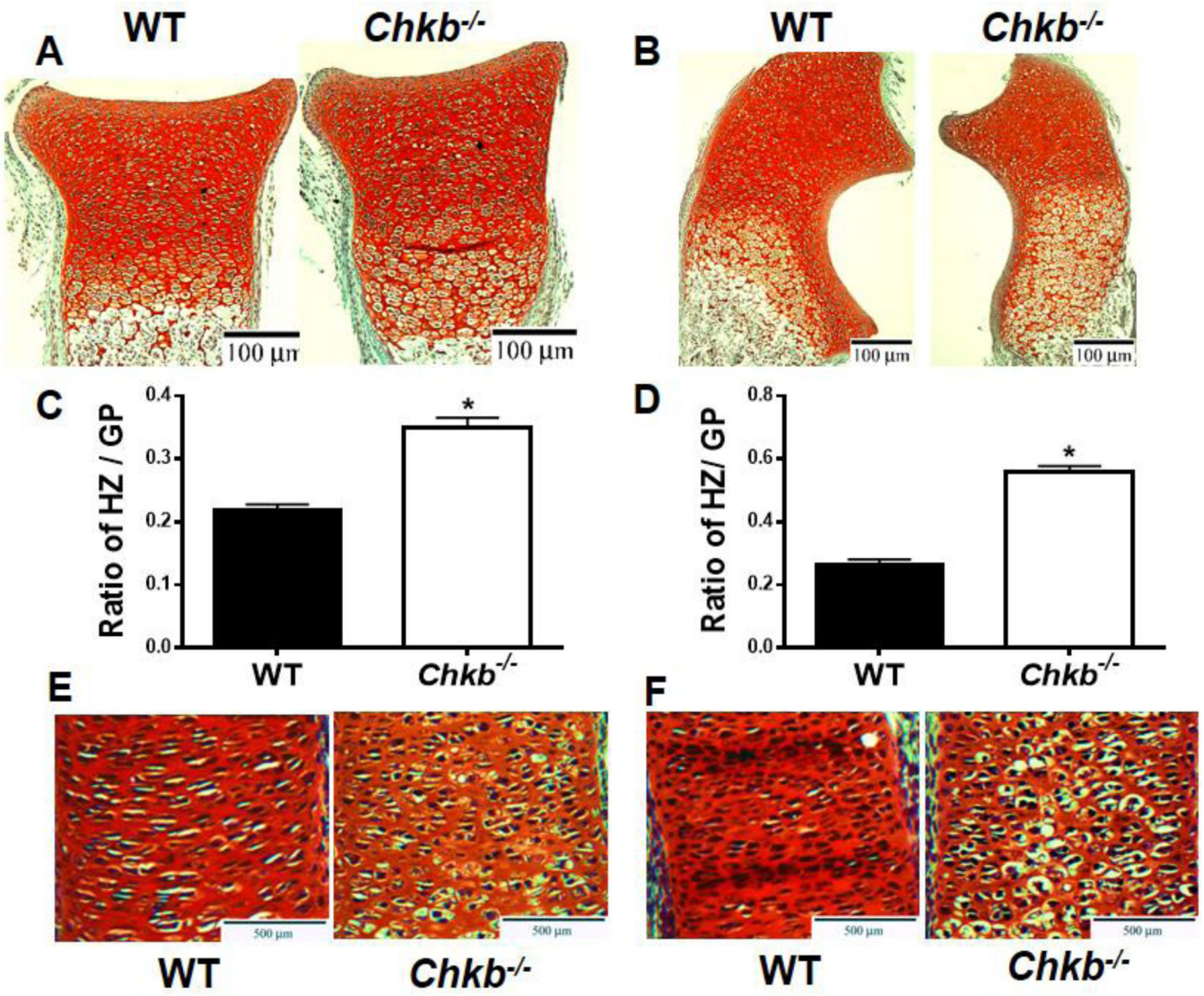

Fig. 3.

Growth plate defects in the radius and ulna of *Chkb*$^{-/-}$ mice. P0 radius (A), P0 ulna (B), E16.5 radius (E) and E16.5 ulna (F) were stained with Safranin O/fast green. The ratio of hypertrophic zone (HZ) length / growth plate (GZ) length is shown in (C, D). Data in (C) and (D) are means ± SEM from 3 littermates of each genotype; *: $P < 0.05$ compared to WT.

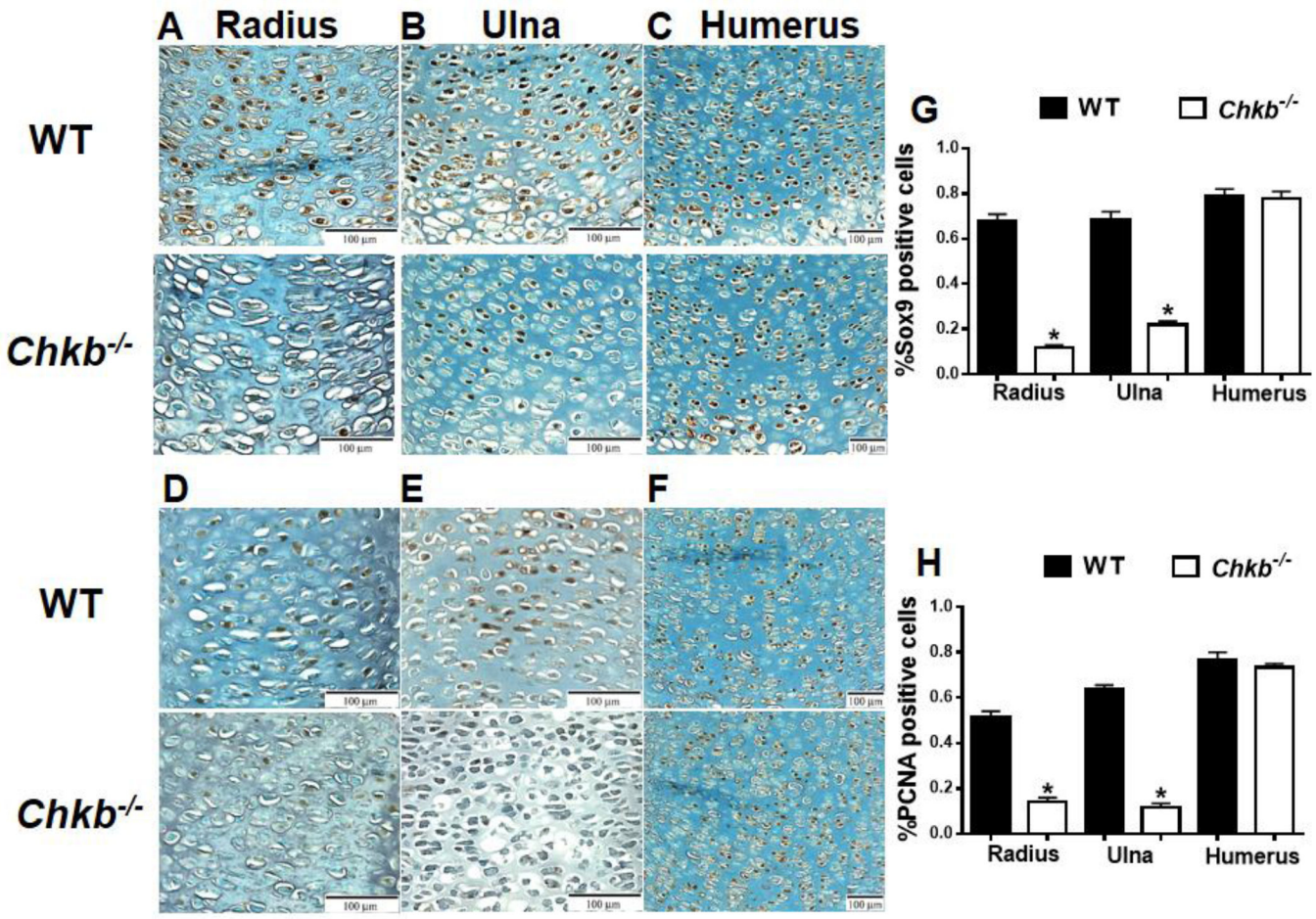

Fig. 4.

Chondrocyte differentiation and proliferation. Chondrocyte differentiation and proliferation were examined in E15.5 embryonic bone growth plates of the radius (A, D), ulna (B, E) and humerus (C, F) of *Chkb*$^{-/-}$ and WT mice by Sox9 (A, B, C) and PCNA (D, E, F) immunohistochemistry. The percentage of positively stained cells was quantified (G, H). Data are means ± SEM from 3–4 littermates of each genotype; *: $P < 0.05$ compared to WT.

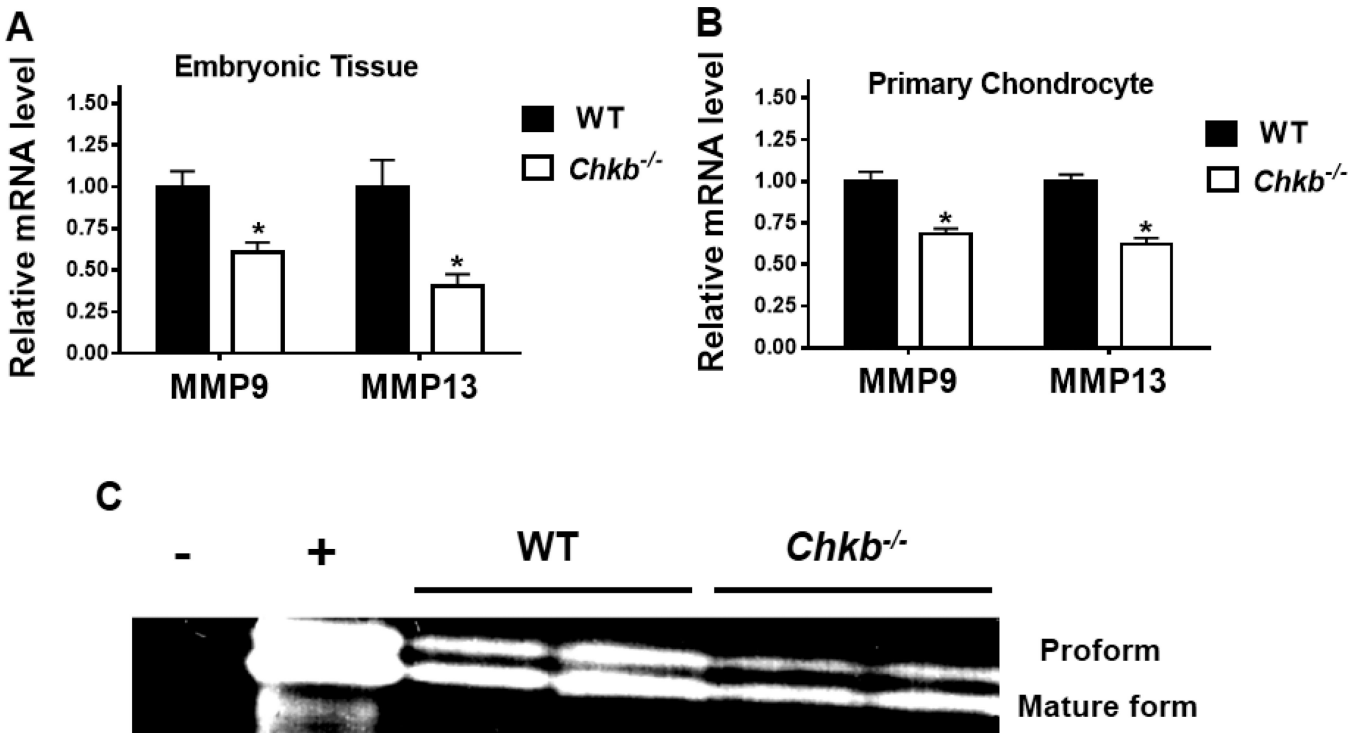

Fig. 5.

mRNA levels and activity of MMPs in the radius and ulna. mRNA levels of MMP9 and MMP13 were analyzed in the radius and ulna of embryonic bone tissues (A) and E15.5 primary chondrocytes (B) of *Chkb*$^{-/-}$ and WT mice by quantitative real-time PCR. Data are means ± SEM from 3 littermates of each genotype; *: $P < 0.05$ compared to WT. (C): MMP9 activity was measured in primary chondrocytes from *Chkb*$^{-/-}$ and WT mice. Gel shows the presence of the proform and the mature form in the gelatin zymography assay. Minus = distilled water (negative control); plus = proteins from the chondrogenic cell line ATDC5 (positive control).

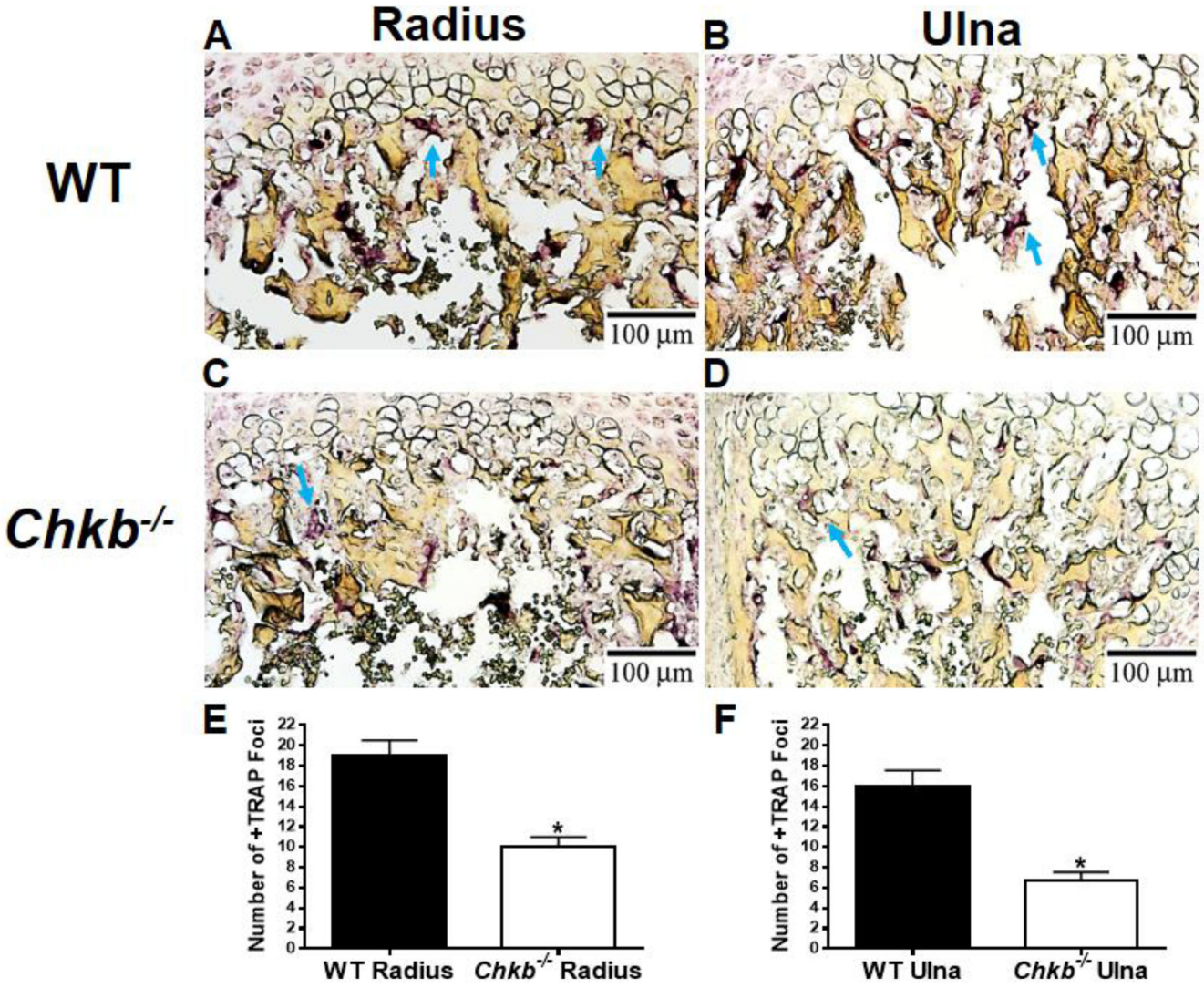

Fig. 6.

The radius and ulna of *Chkb*$^{-/-}$ mice contain fewer osteoclasts along the chondro-osseous junction. Bone sections from the radius (A, C) and ulna (B, D) of 7-day-old WT (A and B) and *Chkb*$^{-/-}$ (C and D) mice were stained for the osteoclast marker, tartrate-resistant acid phosphatase (TRAP). Arrows show dark purple TRAP-positive cells. The number of TRAP-positive foci was quantified along the cartilage/bone interface (E, F). Data are means ± SEM from 3 littermates of each genotype; *: $P < 0.05$ compared to WT.

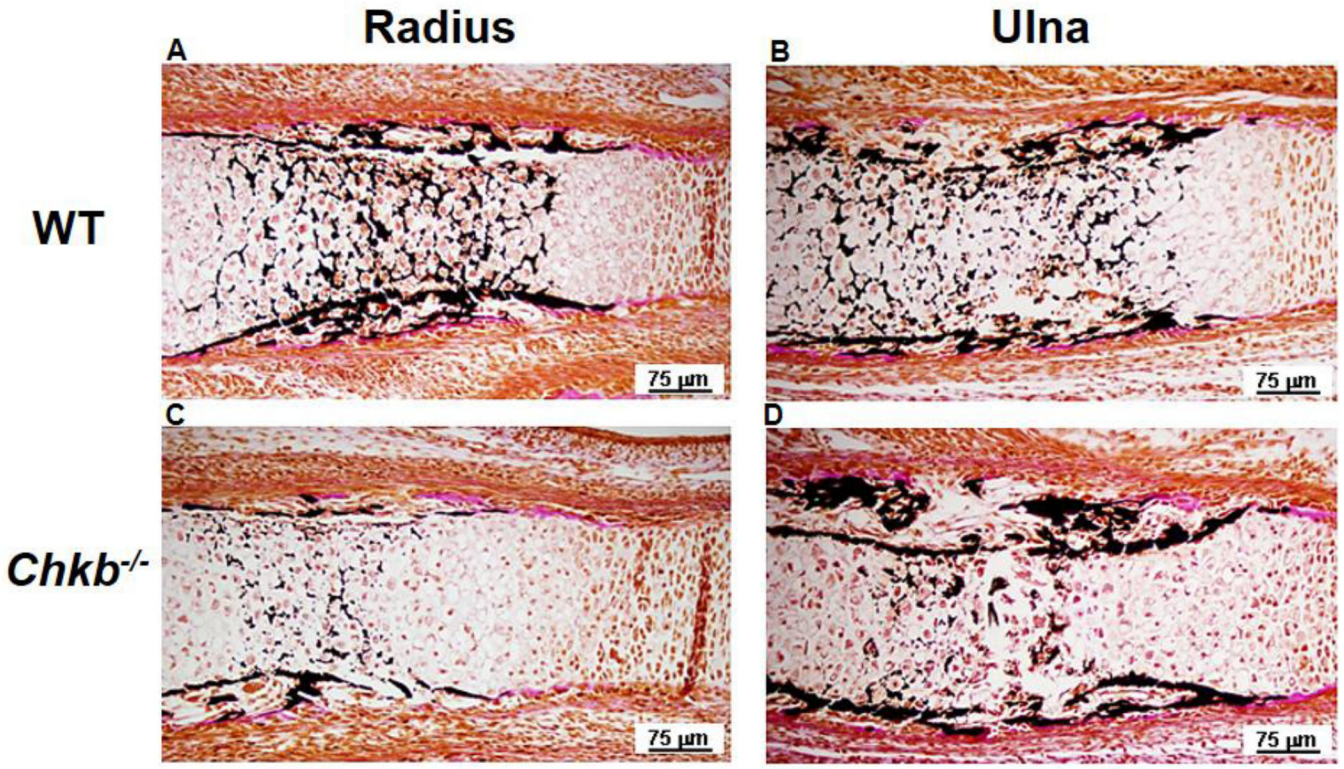

Fig. 7.

Formation of the primary ossification center in the radius and ulna. To evaluate formation of the primary ossification center, radius bones (A, C) and ulna bones (B, D) from E15.5 WT (A, B) and *Chkb*$^{-/-}$ (C, D) mice were stained by the von Kossa method. Dark stain indicates mineralized bone.

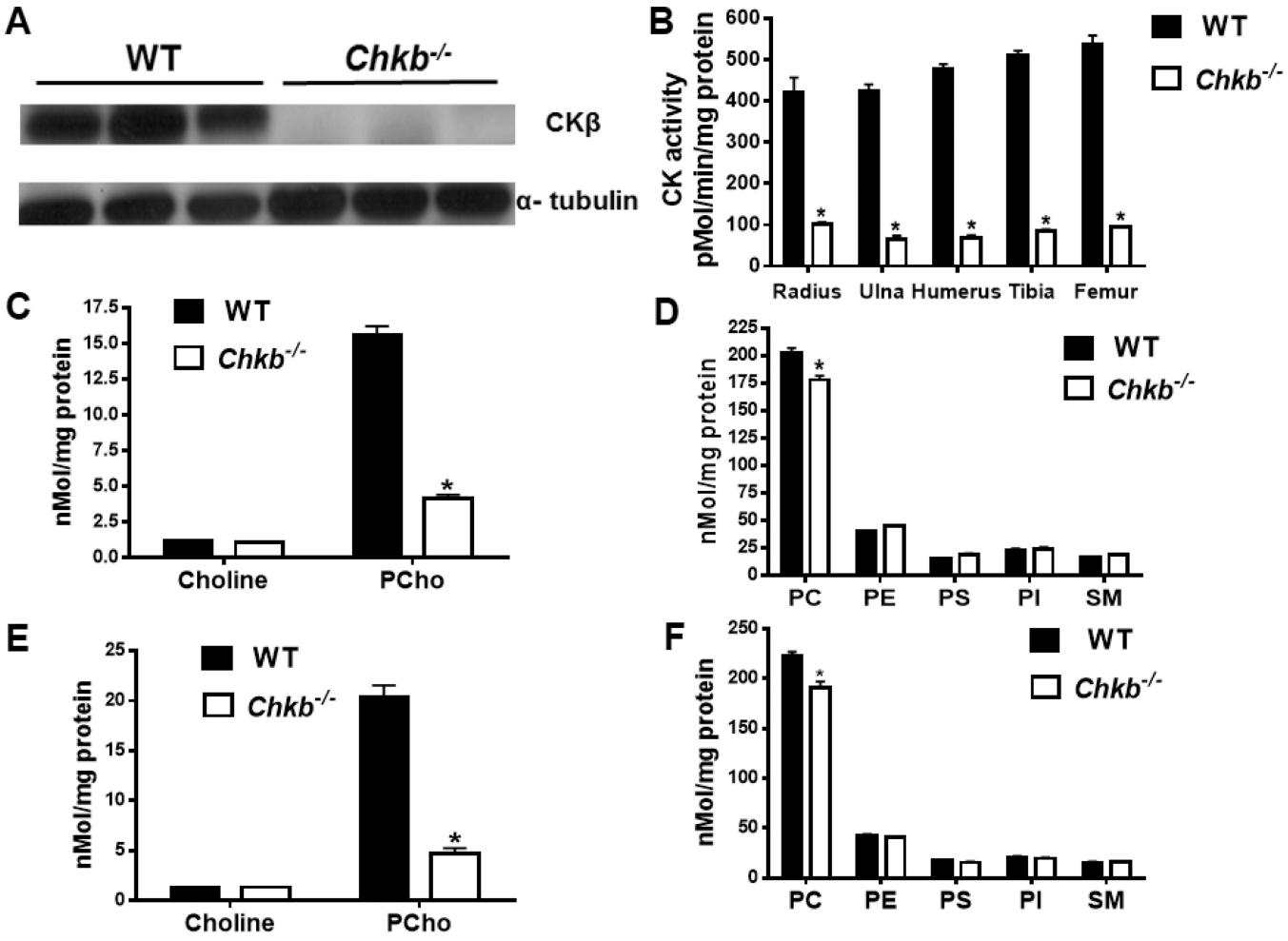

Fig. 8.

Biochemical analyses of primary chondrocytes. E15.5 bones were dissected free of soft tissue and primary chondrocytes were isolated for immunoblotting of CKβ (A), CK enzymatic activity (B), and quantification of choline metabolites (C, E) and phospholipids (D, F) by mass spectrometry. PC, phosphatidylcholine; PE, phosphatidylethanolamine; PS, phosphatidylserine; PI, phosphatidylinositol; SM, sphingomyelin. Data in B-F are means ± SEM from 3 littermates of each genotype; *: $P < 0.05$ compared to WT.